Available online at www.sciencedirect.com
SCIENCE DIRECT®
Polyhedron 25 (2006) 1167–1176
POLYHEDRON
www.elsevier.com/locate/poly

Investigating photoluminescence and electroluminescence of iridium(III)-based blue-emitting phosphors

Inamur R. Laskar, Shih-Feng Hsu, Teng-Ming Chen *

Department of Applied Chemistry, National Chiao Tung University, Hsinchu 30010, Taiwan

Received 9 November 2004; accepted 22 August 2005
Available online 29 September 2005

Abstract

The syntheses of two new cyclometalated ligands [2-(2′,4′-difluorophenyl)-4-*tert*-butylpyridine ($F_2{}^t$Buppy) and 2-(2′,4′-difluorophenyl)-4-oxyhexylpyridine (F_2HexOppy)] were carried out. Blue-light emitting iridium(III) complex dopants [Ir($F_2{}^t$Buppy)$_2$(acac/pic)] (acac = acetylacetone; pic = picolinic acid) and [Ir(F_2HexOppy)$_2$(acac/pic)] were prepared using these cyclometalated ligands with acetylacetone and picolinic acid as their ancillary ligands. The structure of the complexes, [Ir($F_2{}^t$Buppy)$_2$(acac)] and [Ir($F_2{}^t$Buppy)$_2$(pic)] were authenticated by X-ray single-crystal structure analysis and showed an octahedral geometry. Comparative absorption and emission spectra of thin-films as well as their solution samples were studied. The variation of the lowest emitting states to their corresponding unsubstituted complexes, [Ir(F_2ppy)$_2$(acac/pic)] was also discussed. The electroluminescent (EL) device was fabricated using [Ir($F_2{}^t$Buppy)$_2$(pic)] as the dopant (D-**I**) into the emitting layer and compared with two other EL devices where [Ir(F_2MeOppy)$_2$(acac)] (D-**II**) and FIrpic (D-**III**) dopants were used in the same device structure. The lower driving voltages obtained for D-**I** with respect to D-**II** and D-**III** devices were rationalized. The exceptional lowering of the luminance yield of the substituted dopants containing devices, D-**I** and D-**II**, to that of D-**III** which contains the unsubstituted dopant was also investigated.

Keywords: Iridium-complexes; Cyclometalated; Photoluminescence; Crystal-structure; Octahedral; Electroluminescence

1. Introduction

Cyclometalated-based iridium(III) materials are becoming increasingly important to scientists with respect to their applications in light emitting devices [1] due to their high quantum yields of luminescence and electroluminescence, colour tunability, fair stability and straightforward synthetic routes. A significant extent of the tuning of emission wavelengths in the visible range has been performed simply by incorporating electron releasing or withdrawing substituents into the 2-phenyl-pyridine ligand of the iridium(III)–phenyl-pyridine system [1b,2]. Recently, we have reported a similar type of work by attaching an electron releasing methoxy substituent in the pyridyl moiety of the 2-phenyl-pyridine ligand of the corresponding iridium(III) complex [3]. In that work, the tuning of the maximum emission wavelength was performed by employing the electronic property of the substituent, but the electroluminescence (EL) performance of the fabricated device was found to be inferior to that of the corresponding unsubstituted dopant containing EL device. The proper reasons which make such an unexpected lowering of EL quantum yields for the substituted dopant containing device are still unknown. This fact actually motivated us to extend our previous work. Initially, we intended to clarify whether there was any inherent tendency of the dopant with the methoxy-substituted ligand used in the device to be responsible for the observed poor EL efficiency. Two other dopants have been selected, where the pyridyl moiety of 2-phenyl-pyridine contains either a long chain or a branched chain alkyl substituent, which have the same electronic effects. We report the syntheses of Ir(F_2hexO/$F_2{}^t$Buppy)$_2$(acac) and

* Corresponding author. Tel.: +886 5712121x56526; fax: +886 35723764.
E-mail address: tmchen@mail.nctu.edu.tw (T.-M. Chen).

0277-5387/$ - see front matter © 2005 Elsevier Ltd. All rights reserved.
doi:10.1016/j.poly.2005.08.033

$Ir(F_2HexO/F_2{}^tBuppy)_2(pic)$ complexes, their photophysical behaviors and redox properties, the X-ray single-crystal structure analyses of $Ir(F_2{}^tBuppy)_2(acac)$ and $Ir(F_2{}^tBuppy)_2(pic)$ and the applications of $Ir(F_2{}^tBuppy)_2(pic)$ as a dopant in the emitting layer of an EL device.

2. Experiments

2.1. Materials

$IrCl_3 \cdot 3H_2O$ was purchased from Alfa Aesar, USA, 2,4-difluoroboronic acid, picolinic acid, 1-hexanol and glycerol from Aldrich Chemicals, USA, phosphorousoxytrichloride from FERAK Laborat GMBH, Berlin (west), sodium hydride from Lancaster and the rest of the compounds from Tokyo Kasei Kogyo Co. Ltd., Japan, and all materials were used as received.

2.2. Syntheses

2-Chloropyridine-*N*-oxide, 2-chloro-4-nitropyridine-*N*-oxide and 2-chloro-4-nitro pyridine were prepared by following the methods described in the literature [3]. The synthetic routes of the ligands and the complexes are shown in Scheme 1.

2-Chloro-4-oxyhexylpyridine (yield: 53%): 2-Chloro-4-nitropyridine (1 eq) was added to a mixture of dry 1-hexanol (1.1 eq) and sodium hydride (1.5 eq) in dioxane as the solvent. The resulting solution was refluxed for 12 h. The reaction mixture was cooled to room temperature and poured into water. The organic layer separated out and the aqueous layer was washed by ethyl acetate. The combined organic extracts were dried and evaporated to dryness. The compound was purified by column chromatography. ^1H NMR (300 MHz, $CDCl_3$): δ, 8.07 (d, 1H, $J = 5.7$ Hz), 6.93 (d, 1H, $J = 3.0$ Hz), 6.71 (dd, 1H, $J = 2.1$, 6.0 Hz), 3.98 (dd, 2H, $J = 7.3$, 13.5 Hz), 1.72 (m, 2H), 1.45 (m, 2H), 1.25 (m, 4H), 0.82 (m, 3H). EIMS, m/z: 214, calc. 213.5.

2-(2′,4′-difluorophenyl)-4-oxyhexylpyridine (yield 75%): It was prepared by employing the method described in the literature [3]. 2-Chloro-4-oxyhexylpyridine was taken instead of 2-chloro-4-methoxypyridine as the starting material. ^1H NMR (300 MHz, $CDCl_3$): 8.51 (d, 1H, $J = 5.7$ Hz), 7.98 (m, 1H), 7.26 (t, 1H, $J = 2.1$ Hz), 6.94 (m, 2H), 6.78 (dd, 1H, $J = 2.4$, 5.7 Hz), 4.06 (m, 2H), 1.84 (m, 2H), 1.65 (m, 2H), 1.37 (m, 2H), 1.22 (m, 2H), 0.85 (m, 3H). EIMS, m/z: 221, calc. 221.

2-Chloro-4-*tert*-butylpyridine (yield 60%): 4-*tert*-Butylpyridine was chlorinated by the reaction with phosphorousoxytrichloride at low temperature (0–5 °C), it was stirred for 1h at 0 °C and then a further 1h at room temperature (25 °C). Then the reaction mixture was poured slowly into ice-cold water. The product was extracted by ethyl acetate and purified through column chromatography. ^1H NMR (300 MHz, $CDCl_3$): δ, 8.16 (d, 1H, $J = 6.0$ Hz), 7.27 (d, 2H, $J = 5.1$ Hz), 1.21 (s, 9H). EIMS, m/z: 170, calc. 169.5.

2-(2′,4′-Difluorophenyl)-4-*tert*-butylpyridine (yield 72%): This was prepared by a similar method to that described in the literature [3]. ^1H NMR (300 MHz, $CDCl_3$): δ, 8.60 (d, 1H, $J = 5.1$ Hz), 7.94 (dd, 1H, $J = 2.1$, 8.7 Hz), 7.72 (s, 1H), 7.25 (dd, 1H, $J = 1.8$, 5.4 Hz), 6.93 (m, 2H), 1.28 (s, 9H). EIMS, m/z: 247, calc. 247.

$(F_2{}^tBuppyppy)_2Ir(\mu\text{-}Cl)Ir(F_2{}^tBuOppyppy)_2$ (yield 70–75%): A solution of $IrCl_3 \cdot 3H_2O$ (1 mmol) and 2-(2′,4′-difluorophenyl)-4-methoxypyridine (3 mmol) in 2-ethoxyethanol (30 ml) was refluxed for 24 h. The pale green mixture was cooled to room temperature and 20 ml of 1 M HCl was added to precipitate the product. The mixture was filtered and washed with 100 ml of 1 M HCl, followed by 50 ml of methanol and then dried. The prod-

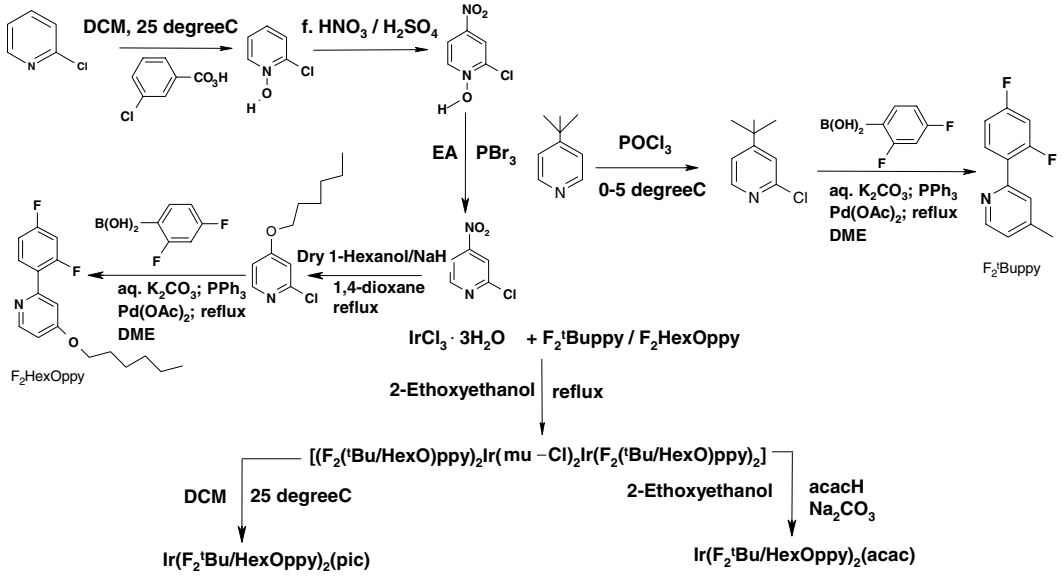

Scheme 1.

uct was obtained as a light green powder. ^{1}H NMR (300 MHz, $CDCl_3$): 9.04 (d, 4H, $J = 6.0$ Hz), 8.33 (s, 4H), 6.87 (d, 4H, $J = 6.0$ Hz), 6.32 (t, 4H, $J = 9.6$ Hz), 5.16 (d, 4H, $J = 7.2$ Hz), 1.58 (s, 36H). FABMS: *m/z*: 1439, fragmented masses, 1403 (–Cl), 1159 (–1 ligand); Calc. 1439.

$(F_2HexOppyppy)_2Ir(\mu\text{-}Cl)Ir(F_2HexOppy)_2$ (yield 70–75%): This has been synthesized by following the same method as described above. ^{1}H NMR (300 MHz, $CDCl_3$): 8.90 (d, 4H, $J = 5.7$ Hz), 7.79 (s, 4H), 6.35 (m, 8H), 5.41 (d, 4H, $J = 7.5$ Hz), 4.21 (d, 8H, $J = 6.0$ Hz), 2.05 (s, 8H), 1.69 (s, 8H), 1.31 (s, 16 H), 0.99 (s, 12H). FABMS: *m/z*: 1615, fragmented masses, 808 (–IrCl(ligand)$_2$), 773 (–Cl), calc. 1615.

$Ir(F_2HexOppy)_2(acac)$ (yield 80%) (**1a**) [1e,4]. $(F_2HexOppy)_2Ir(\mu\text{-}Cl)Ir(F_2HexOppy)_2$ (1 mmol), acetylacetone (3 mmol) and sodium carbonate (10 mmol) were mixed in 10 ml of 2-ethoxyethanol. The mixture was refluxed under nitrogen for 12 h. The reaction mixture was then cooled and the pale green precipitate was filtered off. The product was washed by methanol several times, followed by hexane. Then it was recrystallised from a mixture of dichloromethane and methanol (1:1). ^{1}H NMR (300 MHz, $CDCl_3$): 8.17 (d, 1H, $J = 6.3$ Hz), 7.73 (s, 1H), 6.73 (s, 1H), 6.32 (d, 1H, $J = 11.7$ Hz), 5.72 (d, 1H, $J = 6.0$ Hz), 5.22 (s, 1H), 4.15 (s, 2H), 1.87 (m, 8H), 1.39 (m, 6H), 0.93 (s, 3H). FABMS: *m/z*: 871, fragmented masses, 771 (–acetylacetonate); Calc. 871.

$Ir(F_2{}^tBuppy)_2(acac)$ (yield 80%) (**2a**). This has been prepared by adopting a similar method as described above. ^{1}H NMR (300 MHz, $CDCl_3$): 8.28 (m, 4H), 7.22 (d, 2H, $J = 6.0$ Hz), 6.32 (t, 2H, $J = 10.8$ Hz), 5.66 (d, 2H, $J = 8.4$ Hz), 5.24 (s, 1H), 1.81 (s, 6H), 1.44 (s, 18H), fragmented masses, 684 (–acetylacetonate); FABMS: *m/z*: 783, calc. 783.

$Ir(F_2HexOppy)_2(pic)$ (yield 88%) (**1b**) [1e,4]. 2.2 mmol of picolinic acid was added to a solution of 0.8 mmol of $(F_2{}^tBuppy)_2Ir(\mu\text{-}Cl)Ir(F_2{}^tBuppy)_2$ in 60 ml of dichloromethane at ambient temperature. The mixture was refluxed under nitrogen in an oil bath for 16 h. The reaction mixture was cooled to room temperature and a pale yellow precipitate was filtered off. The pure product was obtained by flash chromatography. ^{1}H NMR (300 MHz, $CDCl_3$): 8.44 (s, 1H), 8.30 (d, 1H, $J = 6.3$ Hz), 7.90 (s, 1H), 7.73 (m, 3H), 7.38 (s, 1H), 7.14 (s, 1H), 6.69 (s, 1H), 6.40 (m, 3H), 5.88 (d, 1H, $J = 8.4$ Hz), 5.65 (d, 1H, $J = 7.8$ Hz), 4.09 (s, 4H), 1.82 (s, 4H), 1.47 (s, 4H), 1.29 (s, 8H), 0.91 (s, 6H). FABMS: *m/z*: 894, fragmented masses, 772 (–picolinate); Calc. 894.

$Ir(F_2{}^tBuppy)_2(pic)$ (yield 92%) (**2b**). This has been synthesized by following the method as described above. ^{1}H NMR (300 MHz, $CDCl_3$): 8.59 (d, 1H, $J = 4.2$ Hz), 8.29 (m, 3H), 8.24 (s, 1H), 7.77 (s, 1H), 7.41 (s, 1H), 7.17 (d, 1H, $J = 4.2$ Hz), 7.00 (d, 1H, $J = 6.0$ Hz), 6.45 (m, 2H), 5.87 (d, 1H, $J = 9.0$ Hz), 5.57 (d, 1H, $J = 8.1$ Hz), 5.30 (s, 1H), 1.38 (s, 18H). FABMS: *m/z*: 806, fragmented masses, 685 (–picolinate), 651 (–Cl); Calc. 806.

$Ir(F_2MeOppy)_2(acac)$ (**3a**) and $Ir(F_2MeOppy)_2(pic)$ (**3b**). The syntheses of these complexes have been described in our previous paper [3].

$Ir(F_2ppy)_2(acac)$ (**4a**) and FIrpic (**4b**). The syntheses of these complexes have also been described previously [5].

2.3. Crystallography

Single-crystal diffraction data for $Ir(F_2{}^tBuppy)_2(acac)$ and $Ir(F_2{}^tBuppy)(pic)$ were collected on a Bruker SmartCCD diffractometer equipped with a normal focus, 3 kW sealed-tube X-ray source ($\lambda = 0.71073$ Å). The intensity data were collected in the ω scan mode (width of 0.3/° frame) and corrected for *Lp* and absorption effects by using the SAINT [6] program. Cell refinement and data reduction were carried out using the program Bruker SHELXTL [7] and the crystal structure was solved by direct methods using the SHELXTL [7] version 5.1 software packages. The structure was further refined by full-matrix least-square methods based on F^2 using SHELXTL version 5.1 [7]. Positions of non-hydrogen atoms were refined anisotropically, whereas the hydrogen positions were not refined.

2.4. Optical measurements and composition analyses

The ultraviolet–visible (UV–Vis) spectra of the phosphorescent iridium(III) complexes were measured on an UV–Vis spectrophotometer (Agilent Model 8453) and corrected for background due to solvent absorption. Photoluminescence (PL) spectra were carried out with a spectrophotometer (Jobin-Yvon Spex, Model Fluorolog-3). Emission quantum yields were measured by the method of Demas and Crosby [8] using *fac*-$Ir(ppy)_3$ as a reference [9]. NMR spectra were recorded on Varian 300 MHz. MS spectra (EI and FAB) were taken by micromass TRIO-2000. Cyclic voltammetry (CV) analyses were performed using CHI 2.05; dichloromethane was used as the solvent in an inert atmosphere and 0.1 M tetra(*n*-butyl)ammonium tetrafluoroborate was used as the supporting electrolyte. A glassy carbon rod was used as the working electrode, platinum was used as the counter electrode, and a silver wire was used as a pseudo-reference electrode. The TG-DTA analysis was carried out using a thermal analyzer (SEIKO 1TG/DTA Model 200). Luminescence lifetimes were obtained by exponentially fitting the emission decay curves recorded on a Continuum Model NY61 spectrofluorometer.

2.5. OLED fabrication and testing

In the fabrication of OLEDs, organic layers were thermally evaporated onto a glass substrate precoated with an indium-tin-oxide (ITO) layer with a sheet resistance of 20 Ω under high-vacuum. Prior to use, the ITO surface was ultrasonicated in a detergent solution followed by rinsing with deionized (DI) water, dipped into acetone, trichloroethylene and 2-propanol, and then degreased with a vapor of 2-propanol. After degreasing, the substrate was

oxidized and cleaned in a UV-ozone chamber before it was loaded into an evaporator. In a vacuum chamber at a pressure of 10^{-6} Torr, different layers (discussed in the EL discussion) were sequentially deposited onto the substrate to give the device structure. The current–voltage (*I–V*) profiles and light intensity characteristics for the above-fabricated devices were measured in a vacuum chamber of 10^{-6} Torr at ambient temperature using a Keithley 2400 Source Meter/2000 Multimeter coupled to a PR 650 Optical Meter.

3. Results and discussion

3.1. Syntheses

The syntheses of two new cyclometalated ligands, 2-(2′,4′-difluorophenyl)-4-oxyhexylpyridine and 2-(2′,4′-difluorophenyl)-4-*tert*-butylpyridine were carried out. The incorporation of an oxyhexyl group into the pyridyl moiety of 2-(2′,4′-difluorophenyl)-4-pyridine follows an almost similar method as described previously [3], except for step 4, where the nitro substituent was replaced by using dry 1-hexanol and sodium hydride as the base. The oxyhexyl substituent was incorporated into the pyridyl moiety of 2-(2′,4′-difluorophenyl)-4-pyridine in six steps, whereas the *tert*-butyl substituent just took two steps. Syntheses of cyclometalated complexes of iridium(III) were performed as described previously [3] using the oxyhexyl/*tert*-butyl-substituted ligands as the cyclometalated ligands and acetylacetone/picolinic acid as ancillary ligands. The thermogravimetric analysis of these complexes showed that the picolinate-Ir complexes are more stable than their corresponding acetylacetonate analogues (decomposition temperature (T_d): **1a**, 268 and **1b** 370; **2a**, 290 and **2b**, 310; **4a**, 216 and **4b** 344 °C) (Fig. 1). It is assumed that the free oxygen atom present in the picolinate of the Ir–picolinate complexes is responsible for making strong intermolecular H-bonding and hence increases the decomposition temperature. This fact is supported by the H-bonding obtained from the crystal structure of **1b**, i.e., O2···H1A′-C1A′ 2.607 Å and 120°.

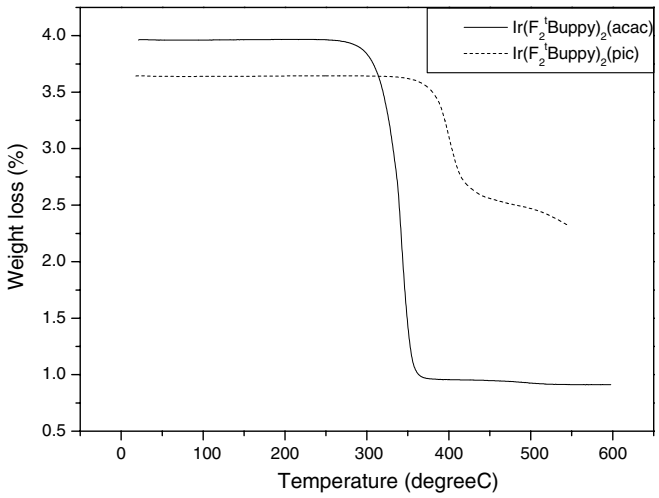

Fig. 1. Thermogravimetric analysis shows the decomposition temperature of [Ir(F_2′Buppy)$_2$(acac)] (**2a**) and [Ir(F_2′Buppy)$_2$(pic)] (**2b**).

3.2. Description of the X-ray structures

ORTEP plots of (F_2′Buppy)$_2$Ir(acac) and (F_2′Buppy)$_2$Ir(pic) molecules are shown in Fig. 2(a) and (b), respectively. Crystallographic data are given in Table 1, and selected bond lengths (Å) and angles (°) for these complexes are presented in Table 2. Single crystals of (F_2′Buppy)$_2$Ir(pic) were of lower quality than those of (F_2′Buppy)$_2$Ir(acac), which is reflected in the poor agreement factor for the (F_2′Buppy)$_2$Ir(pic) complex (Table 1). Both the complexes have octahedral geometry around iridium with *cis*-C,C *trans*-*N*,*N* chelate disposition. The Ir–C and Ir–N bond lengths are within the normal ranges expected for cyclometalated iridium(III) complexes [1b,4]. The Ir–O bond lengths are longer than the mean value of 2.088 Å reported in the Cambridge Crystallographic Database and reflect the large *trans* influence of the phenyl groups. All other bond lengths and angles within the chelate ligands are typical for cyclometalated complexes with ppy and acac/pic ligands bound to iridium(III) [2c,4,10].

3.3. Photoluminescence spectra

Fig. 3(a) and (b) shows mainly the lowest energy absorption bands for the acetylacetonate and picolinate analogues, respectively. The bands observed in the range 350–440 nm can be assigned as intraligand (IL) (π–π*) transitions (ppy^-) and metal-to-ligand charge-transfer (^{1}MLCT) (dπ (Ir) → π* (ppy^-)) transitions. Additionally, the spectra of all these complexes exhibit weaker absorption tails towards lower energy regions (440–480 nm), which may be attributed to triplet metal-to-ligand charge-transfer transitions (^{3}MLCT). As observed in Fig. 3(a) and (b), the picolinate analogues show significantly higher MLCT transitions with respect to their corresponding acetylacetonate analogues. If the comparison is confined to a particular series of complexes, either picolinate or acetylacetonate, the trend of blue-shifting of MLCT states is as follows: unsubstituted complex (FIrpic) < *tert*-butylsubstituted complex < methoxy-substituted complex ∼ oxyhexyl-substituted complex. The observed shift toward higher energy indicates an increase in energy separation between the metal d- and π*-orbitals and the strong electron-releasing effects of the substituents raise the π* orbitals of the cyclometalated ligand. These lowest excited states show solvatochromic effects and are shifted hypsochromically with increasing polarity of the solvents. As shown in Fig. 4(a), the decreasing order of maximum emission wavelength of a thin-film acetylacetonate sample is as follows: **1a** = **3a** > **2a** > **4a**. The same trend has also been observed in the picolinate thin-film analogues (Fig. 4(b)). The results reveal that the strongest electron releasing substituents, methoxy and oxyhexyl groups, shift the emission wave-

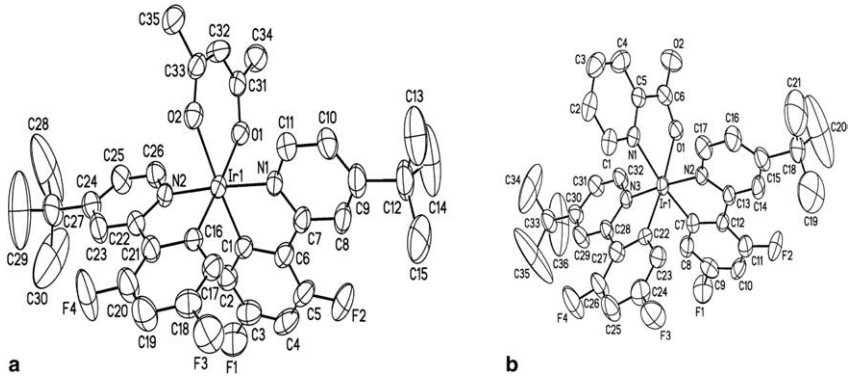

Fig. 2. ORTEP diagrams of: (a) [Ir(F_2'Buppy)$_2$(acac)] (**2a**) and (b) [Ir(F_2'Buppy)$_2$(pic)] (**2b**) (showing 50% thermal probability).

Table 1
Crystal data and structure refinement for Ir(F_2'Buppy)$_2$(acac) and Ir(F_2'Buppy)$_2$(pic)

Compound	Ir(F_2'Buppy)$_2$(acac)	Ir(F_2'Buppy)$_2$(pic)
Empirical formula	$C_{35}H_{35}F_4IrN_2O_2$	$C_{36}H_{32}F_4IrN_3O_2$
Formula weight	783.85	806.85
T (K)	294(2)	294(2)
λ (Å)	0.71073	0.71073
Crystal system	monoclinic	monoclinic
Space group	$P2_1/n$	$P2_1/n$
Unit cell dimensions		
a (Å)	13.6202(9)	13.7196(7)
b (Å)	11.7089(8)	11.6424(6)
c (Å)	20.9951(14)	21.3823(12)
β (°)	96.374(1)	95.671(1)
V (Å^3)	3327.5(4)	3398.7(3)
Z	4	4
D_{calc} (Mg m^{-3})	1.565	1.577
Absorption coefficient (mm^{-1})	4.067	3.986
F(000)	1552	1592
Crystal size (mm^3)	$0.51 \times 0.28 \times 0.20$	$0.2 \times 0.18 \times 0.1$
θ Range for data collection (°)	1.70–28.29	1.69–25.09
Index ranges	$-17 \leqslant h \leqslant 13$, $-15 \leqslant k \leqslant 15$, $-27 \leqslant l \leqslant 28$	$-8 \leqslant h \leqslant 16$, $-13 \leqslant k \leqslant 13$, $-25 \leqslant l \leqslant 25$
Reflections collected	20733	18104
Independent reflections (R_{int})	7801 (0.0360)	6031 (0.0647)
Completeness to θ (%)	94.4 (28.29 °)	99.9 (25.09 °)
Absorption correction	empirical	empirical
Maximum and minimum transmission	0.94343 and 0.50276	0.96364 and 0.75732
Refinement method	full-matrix least-squares on F^2	full-matrix least-squares on F^2
Data/restraints/parameters	7801/0/397	6031/0/415
Goodness-of-fit on F^2	1.318	1.308
Final R indices [$I > 2\sigma(I)$]	$R_1 = 0.0490$, $wR_2 = 0.0916$	$R_1 = 0.0746$, $wR_2 = 0.1328$
R indices (all data)	$R_1 = 0.0569$, $wR_2 = 0.0941$	$R_1 = 0.0956$, $wR_2 = 0.1385$
Largest difference in peak and hole (e Å^{-3})	1.403 and −2.300	1.654 and −2.643

length to the most blue region (458 nm), followed by the *tert*-butyl (462 nm) and then the unsubstituted (466 nm) complexes. This fact indirectly supports that the positions of the substituents in the ligand (pyridyl moiety) contains the LUMO states for these complexes. It also corroborate that the oxy-alkyl substituents exert stronger electronic effects relative to that of *tert*-butyl substituent. The shifting of the maximum emission wavelength is independent of the chain lengths of –OCH_3 and –O–CH_2–$(CH_2)_4$–CH_3 substituents. Solution PL emission spectra of the acetylacetonate analogues show the same trend of shifting emission wavelength (Fig. 5(a)) as is observed for the thin-film samples (Fig. 4(a)), while a different trend is observed for the solution picolinate complexes, i.e., **2b** > **4b** > **3b** > **1b** (Fig. 5(b)). The solution spectra of the oxy-alkyl substituted complexes show red-shifted and broad emission spectra relative to that of their thin-film samples. This observation prompted us to study the emissive characteristics of all the available acetylacetonate and picolinate complexes in different solvents with increasing polarities, that is systematic changes in polarity. Hence, the measurement of the solution emission spectra of these complexes were conducted in the following solvents of different polarities, toluene < chloroform < acetone < acetonitrile < methanol.

Table 2
Selected bond distances (Å) and bond angles (°) for Ir(F_2'Buppy)$_2$(acac) and Ir(F_2'Buppy)$_2$(pic)

Ir(F_2'Buppy)$_2$(acac)		Ir(F_2'Buppy)$_2$(pic)	
Ir(1)–C(16)	1.982(5)	Ir(1)–C(22)	1.987(10)
Ir(1)–C(1)	1.994(5)	Ir(1)–C(7)	2.003(10)
Ir(1)–N(2)	1.026(4)	Ir(1)–N(2)	2.032(8)
Ir(1)–N(1)	2.035(4)	Ir(1)–N(3)	2.036(8)
Ir(1)–O(1)	2.141(4)	Ir(1)–N(1)	2.146(9)
Ir(1)–O(2)	2.151(4)	Ir(1)–O(1)	2.148(7)
C(16)–Ir(1)–C(1)	91.0(2)	C(22)–Ir(1)–C(7)	89.9(4)
C(16)–Ir(1)–N(2)	80.83(19)	C(22)–Ir(1)–N(2)	96.6(4)
C(1)–Ir(1)–N(2)	96.9(2)	C(7)–Ir(1)–N(2)	79.9(4)
C(16)–Ir(1)–N(1)	96.24(19)	C(22)–Ir(1)–N(3)	80.3(4)
C(1)–Ir(1)–N(1)	81.0(2)	C(7)–Ir(1)–N(3)	98.1(4)
N(2)–Ir(1)–N(1)	176.42(17)	N(2)–Ir(1)–N(3)	176.2(3)
C(16)–Ir(1)–O(1)	176.61(18)	C(22)–Ir(1)–N(1)	97.0(4)
C(1)–Ir(1)–O(1)	89.84(18)	C(7)–Ir(1)–N(1)	172.4(4)
N(2)–Ir(1)–O(1)	95.81(16)	N(2)–Ir(1)–N(1)	95.9(3)
N(1)–Ir(1)–O(1)	87.13(16)	N(3)–Ir(1)–N(1)	86.5(3)
C(16)–Ir(1)–O(2)	91.28(18)	C(22)–Ir(1)–O(1)	173.5(4)
C(1)–Ir(1)–O(2)	176.30(18)	C(7)–Ir(1)–O(1)	96.2(3)
N(2)–Ir(1)–O(2)	86.33(16)	N(2)–Ir(1)–O(1)	86.7(3)
N(1)–Ir(1)–O(2)	95.84(16)	N(3)–Ir(1)–O(1)	96.6(3)
O(1)–Ir(1)–O(2)	88.04(14)	N(1)–Ir(1)–O(1)	77.1(3)

The solution spectra of the picolinate complexes are highly affected by the solvent polarity (Fig. 6(a)–(d)). In general, the broad and red-shifted emission is observed with increasing order of polarity. Again, the oxy-alkyl subsitituted complexes are mostly affected by solvents followed by the *tert*-butyl substituted and the unsubstituted complexes. The emission profile of the acetylacetonate complexes, however, remains almost unaffected (Fig. 7(a) and (b)). Presumably, the lowest excited state of the Ir–picolinate complexes has a significant contribution from the excited states of picolinate which is highly affected by solvent polarity. The PL quantum yields were obtained relative to [Ir(ppy)$_3$] ($\phi_{PL} = 0.4$) and the maximum value were found for the Ir(F_2'Buppy)$_2$(acac) complex (Table 3).

3.4. Cyclic voltametric studies

Analysis by cyclic voltammetry shows that all these acetylacetonates and picolinates undergo a reversible one-electron oxidation; no reduction processes were observed in chloroform. As shown in Table 3, the oxidation potentials are slightly affected by the type of ancillary ligand (acetylacetonate and picolinate; ~125 mV) for each pair of complexes, but they vary significantly between complexes with different substitutions (*tert*-butyl and oxyhexyl; ~350 mV). Oxyhexyl-substituted complexes show lower oxidation potentials with respect to their corresponding *tert*-butyl-substituted analogues, indicating the relative ease of oxidation.

3.5. Electroluminescence

The electroluminescent (EL) properties of the complex **2b** were investigated. The EL device performance was investigated by using **2b** as a dopant and CBP [4,4′-bis(9-carbazolyl)-1,1′-biphenyl] as the host in the emitting zone (D-**I**). The device structure adopted in this work is a typical multi-layer, employing indium tin oxide (ITO) as the anode, polyfluoro carbon (CF_x) as the hole injecting material, 4,4′-bis[(1-naphthyl)(phenyl)amino]-1,1-biphenyl (NPB) as the hole transporting material, **2b** as the dopant and CBP as the host, 2,6-dimethyl-4,7-diphenyl-1,10-phenanthroline (BCP) as the hole blocking material, aluminium *tris*(8-quinolinolate) (Alq_3) as the electron-transport material, LiF as the electron-injection layer and aluminum as the cathode, as shown in Fig. 8 (inset). The complex emits a greenish-blue emission in the EL spectra (Fig. 8), which are well matched to that observed in the PL spectra in solution. There are no characteristic emission peaks from Alq_3 or CBP, except a very weak emission from the NPB layer (weak emission ~425 nm in Fig. 8), indicating the emission originates from the dopant in the emitting layer. Furthermore, these results support that the effective energy transfer from the host (CBP) to the dopant (Ir complex) occurs in the emissive layer. The fabrication of another two devices

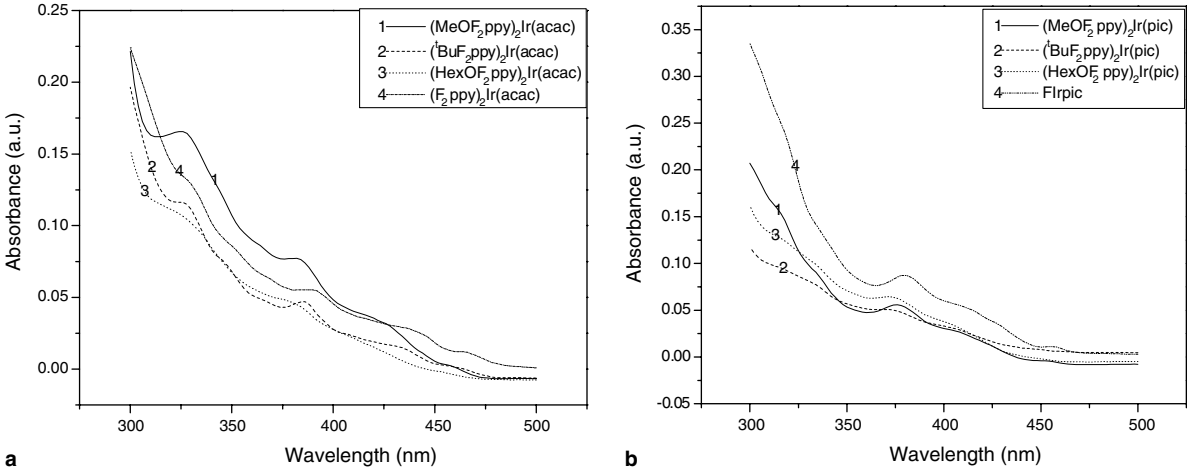

Fig. 3. Comparative absorbance spectra of the series of acetylacetonate (a) and picolinate (b) iridium(III) complexes.

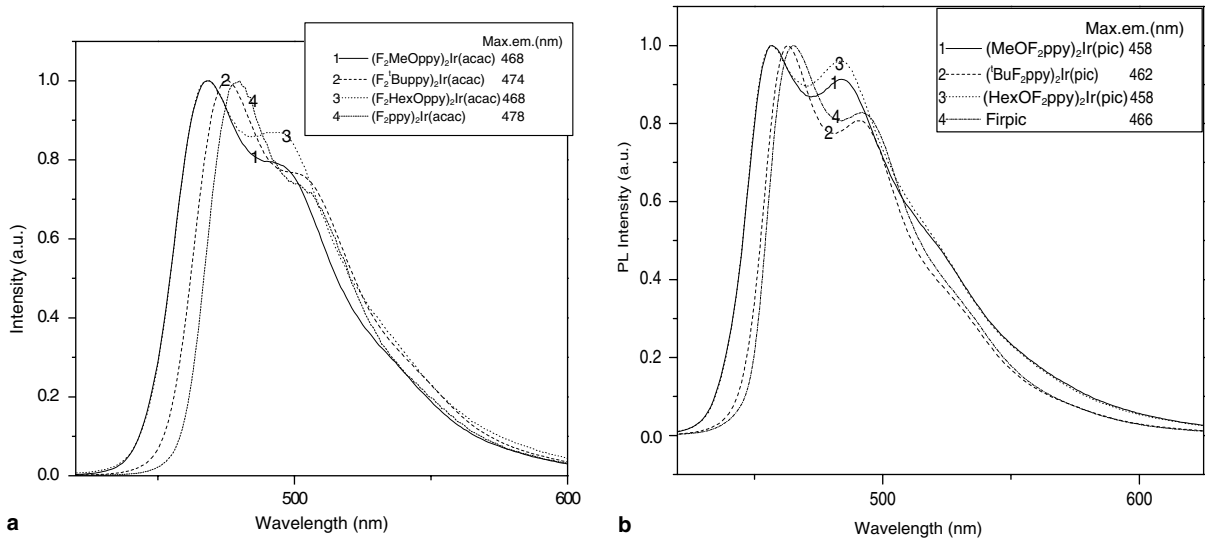

Fig. 4. Solid thin-film emission spectra of the series of acetylacetonate (a) and picolinate (b) iridium(III) complexes.

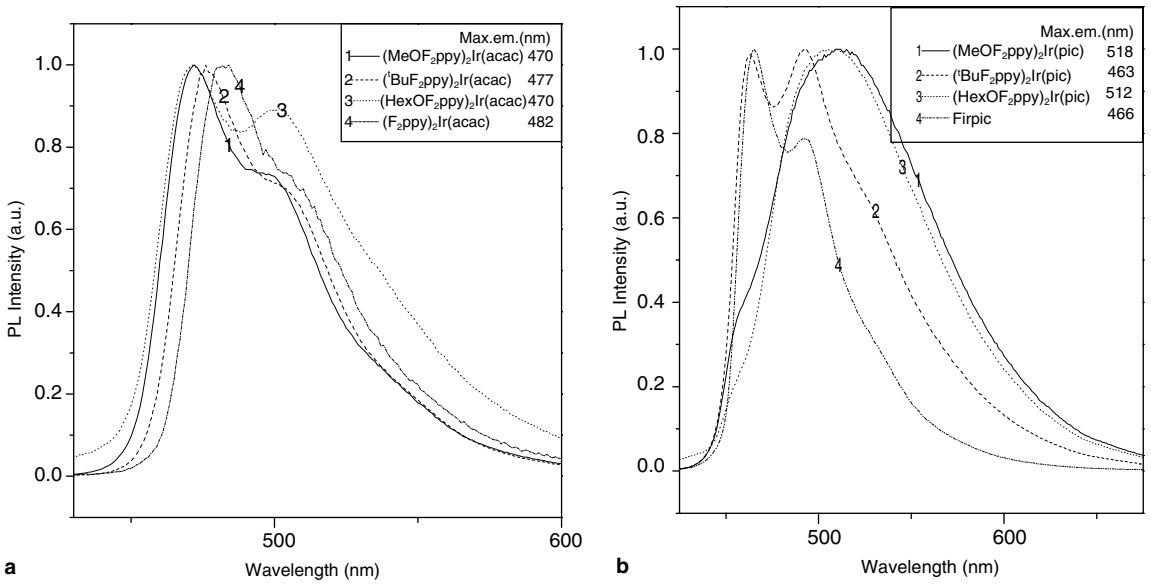

Fig. 5. Solution emission spectra (chloroform) of the series of acetylacetonate (a) and picolinate (b) iridium(III) complexes.

was also carried out, using $Ir(F_2MeOppy)_2(acac)$ [3] (D-**II**) and FIrpic (D-**III**), **3** dopants in a similar device structure as mentioned above to make a comparative study of EL performances. The lowest unoccupied molecular orbitals (LUMO) primarily lie on the pyridyl moiety [11] of the cyclometalated ligand in **2b** and it contains the electron releasing substituent *tert*-butyl (^{t}Bu). The electronic effect of the *tert*-butyl (^{t}Bu) substituent in the pyridyl moiety uplifts the LUMO state and a hypsochromically shifted emission is observed subsequently with respect to the unsubstituted Firpic complex in EL emission (472 nm → 468 nm; Fig. 8). The EL device containing the dopant $Ir(F_2MeOppy)_2(acac)$ shows the maximum emission at 472 nm, where the ancillary ligand (acac) is different from that of FIrpic and **2b**. The turn-on voltages of D-**I**, D-**II** and D-**III** are 5.6, 5.9 and 6.9, respectively (Fig. 9). The intermolecular interactions (e.g., π–π stacks in the molecular crystals) in the solid state and the ability to trap charges in the emissive layer are considered to be the most important factors in determining the operating voltage. The strong electronic coupling and intermolecular interactions in the molecular crystals contribute to effective injections and transport of charges, leading to lower operating voltages [12]. On the other hand, effective charge-trapping by the dopants gives rise to increasing driving voltages in OLEDs [13]. If the dopant material functions as a hole trap, the HOMO level of the dopant could be above that of the host material. Hence, materials having a lower oxidation potential can function as effective hole traps in OLEDs. Therefore, the observed higher operating voltages for D-**III** relative to D-**I** are predominantly caused due to effective hole trapping, which is consistent with the electro-

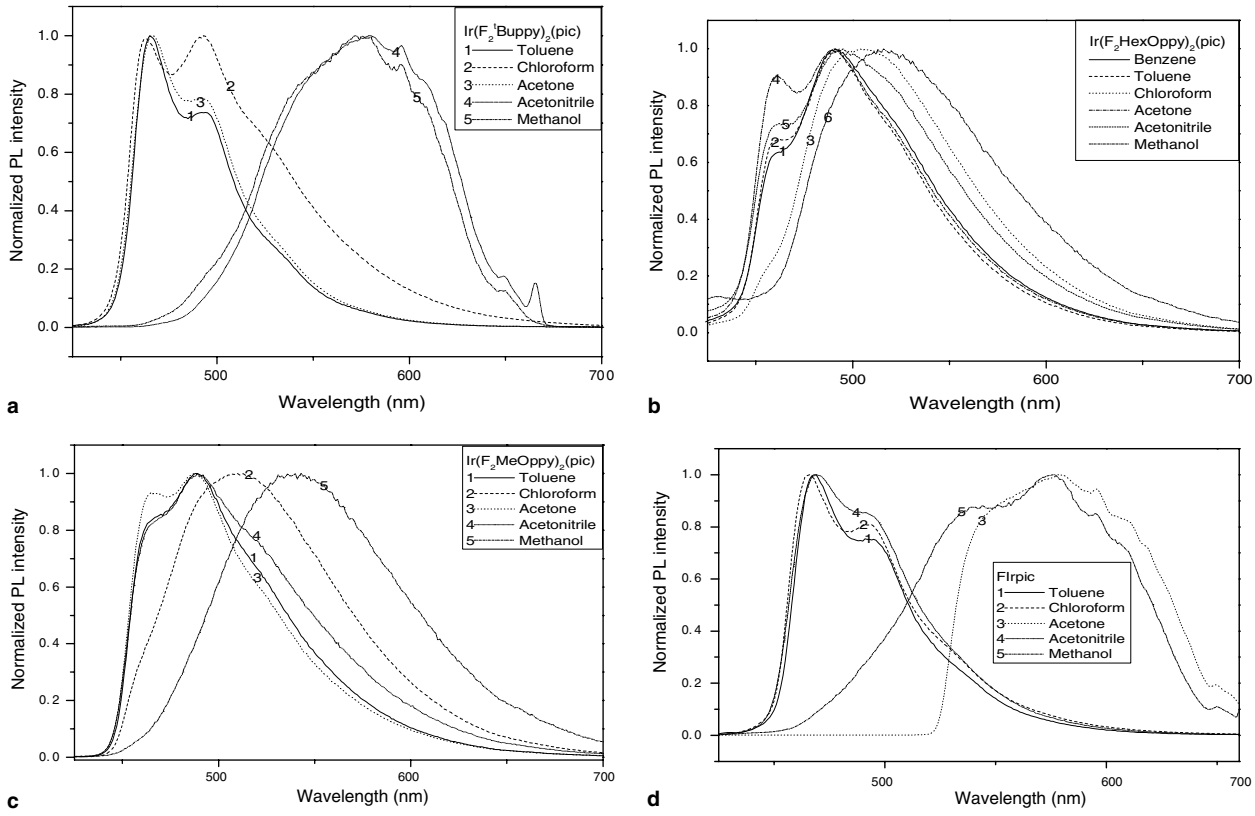

Fig. 6. Solvent dependent emission spectra of the iridium(III)-picolinate complexes: [Ir(F_2'Buppy)$_2$(pic)] (shown in a), [Ir(F_2HexOppy)$_2$(pic)] (shown in b), [Ir(F_2MeOppy)$_2$(pic)] (shown in c) and [Ir(F_2ppy)$_2$(pic)] (shown in d).

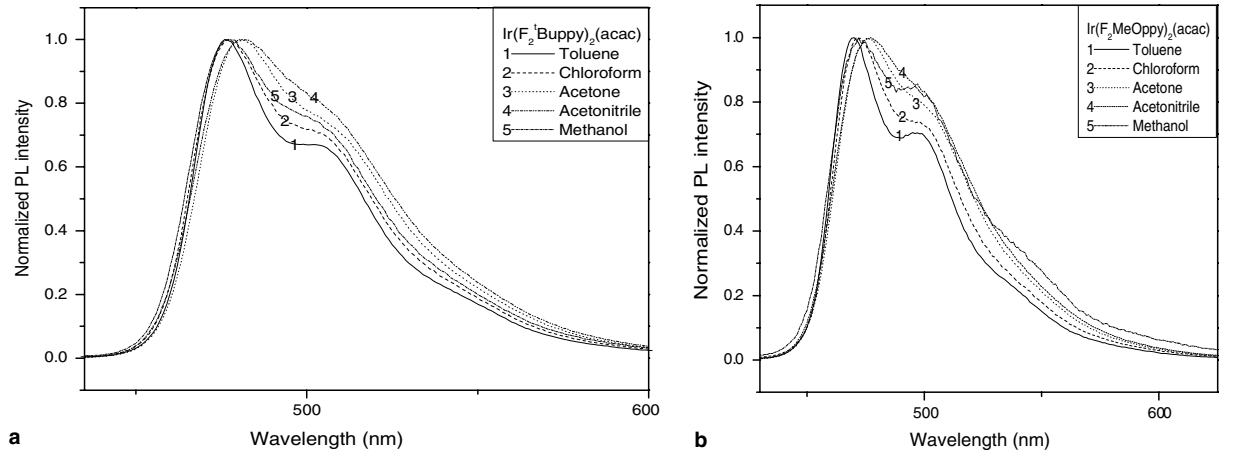

Fig. 7. Solvent dependent emission spectra of the iridium(III)-acetylacetonate complexes: [Ir(F_2'Buppy)$_2$(acac)] (shown in a) and [Ir(F_2'Buppy)$_2$(acac)] (shown in b).

chemical behavior of the dopants used in these devices (i.e., E^{ox} of **2b** (dopant in D-**I**) 0.866 V; E^{ox} of FIrpic (dopant in D-**III**) 0.586 V). The electrochemical behavior of the dopant used in D-**II** (E^{ox} of Ir(F_2MeOppy)$_2$(acac) (dopant in D-**II**) 0.506 V) is almost similar to that of D-**III**, but the observed operating voltage is significantly smaller than that of D-**III**. Presumably, the dopant used in D-**II** has relatively strong intermolecular interactions (MeO-substituent present; π–π stacks) as compared to that of the dopant used in D-**III**, which is responsible for better injection of charges and hence correspondingly lowering of driving voltages. The comparative EL performances of the devices are shown in Table 4. The luminance yield for D-**III** is superior to the remaining devices described herein. Poor solution PL luminance yield is observed (Table 3) for the substituted dopants relative to that of FIrpic, reflecting the comparatively poor EL luminance yield observed for D-**I** and **II** devices. These experiments further prompt us that there is no

Table 3
Photophysical and electrochemical data for the acetylacetonate and picolinate analogues of the iridium(III) complexes

Complex	Absorbance[a] λ (nm) ($\log\varepsilon$)	Emission λ_{max} (nm)		Quantum efficiency[a,c]	Redox $E^{ox}_{1/2}$ (V)[a]	Band gap (eV)
		Solution[a,b]	Film[b]			
$Ir(F_2{}^tBuppy)_2(acac)$	386 (4.7); 464 (4.2)	477	474	0.86	0.746	2.55
$Ir(F_2{}^tBuppy)_2(pic)$	375 (4.7); 454 (4.3)	463	462	0.78	0.866	2.77
$Ir(F_2HexOppy)_2(acac)$	379 (4.7); 456 (4.3)	470	468	0.48	0.391	2.71
$Ir(F_2HexOppy)_2(pic)$	373 (4.7); 441 (4.5)	512	458	0.71	0.504	2.72

[a] Solvent used dichloromethane.
[b] Excitations used 383, 377, 381 and 369 nm for solutions and 285, 276, 278 and 277 nm for thin films.
[c] Values are reported relative to $Ir(ppy)_3$.

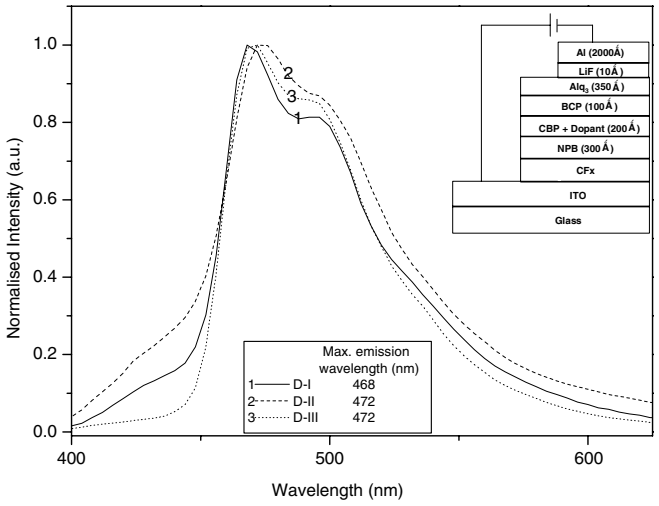

Fig. 8. Comparative EL emission spectra of the devices, D-**I**, D-**II** and D-**III**.

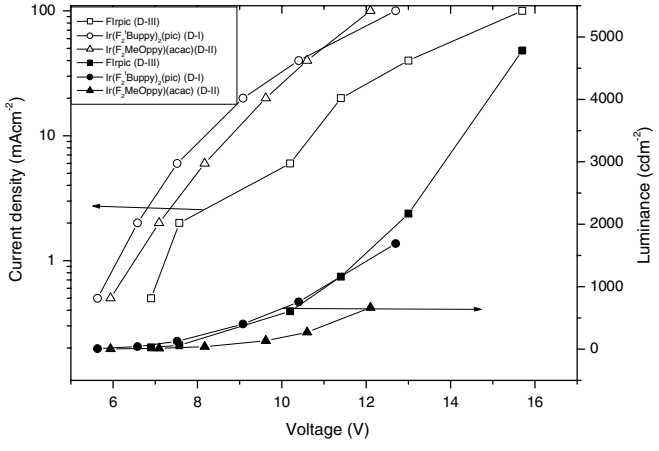

Fig. 9. Comparative current density–voltage–luminance (*I–V–L*) curves of the devices, D-**I**, D-**II** and D-**III**.

inherent tendency of the substituted dopants which results in abnormal worsening of EL performances.

Assuming that the emitting state of a complex is formed with unit efficiency, based on the $k_r = \phi_{PL}/\tau$ and $\phi_{PL} = k_r/(k_r + k_{nr})$ relationships, the calculations of radiative (k_r) and non-radiative (k_{nr}) rate constants of $Ir(F_2{}^tBuppy)_2(acac)$ ($\phi_{PL} = 0.78$; $\tau = 0.11$ μs; $k_r = 7.1 \times 10^6$; $k_{nr} = 2.0 \times 10^6$), $Ir(F_2MeOppy)_2(acac)$ ($\phi_{PL} = 0.60$; $\tau = 0.097$ μs; $k_r = 6.2 \times 10^6$; $k_{nr} = 4.0 \times 10^6$) and FIrpic ($\phi_{PL} = 0.99$; $\tau = 0.11$ μs; $k_r = 9 \times 10^6$; $k_{nr} = 9 \times 10^4$) were performed. The radiative rate constants for these complexes show almost similar order (10^6), but the non-radiative rate constants for FIrpic are less than two orders of magnitude smaller than those of substituted dopants. The non-radiative rate constant is a sum of rates for several processes that quench emission. It appears that a new luminescent quenching mechanism comes into play as the energy of the triplet states increases (for the case of substituted dopants). It may involve a self-quenching mechanism or perhaps thermal activation to a competing MLCT state on the ancillary ligand.

4. Conclusion

Syntheses of new blue-emitting iridium(III) based phosphorescent materials have been carried out. Systematic changes of emission wavelengths have been demonstrated by various ligands with different electronic properties to form a series of Ir complexes. Solution photoluminescence behavior of iridium(III)-acetylacetonate/picolinate complexes were also investigated. Comparative EL performances were also examined using three similar types of dopants described herein with the same device configuration, and the observed poor device performances for the device containing a substituted dopant with respect to the device which contains a dopant without a substituent was rationalized.

Table 4
Comparative EL performances for devices D-**I**, **II** and **III**

Dopants used (Device)	Current density (mA cm^{-2})	Drive voltage (V)	Luminance (cd m^{-2})	Luminance yield (cd A^{-1})	CIE		λ_{max} (nm)	Quantum efficiency (%)
					x	*y*		
$(F_2{}^tBuppy)_2Ir(pic)$ (D-**I**)	20	9.1	402	2.0	0.17	0.30	468	1.0
$(F_2MeOppy)_2Ir(acac)$ (D-**II**)	20	9.6	133	0.7	0.19	0.31	472	0.4
FIrpic (D-**III**)	20	11.4	1161	5.8	0.16	0.32	472	3.3

5. Supplementary material

Crystallographic data for the structural analysis have been deposited with the Cambridge Crystallographic Data Centre, CCDC Nos. 253380 and 253381 for compounds $Ir(F_2{}^tBuppy)_2(acac)$ and $Ir(F_2{}^tBuppy)(pic)$, respectively. Copies of this information may be obtained free of charge from the Director, CCDC, 12 Union Road, Cambridge, CB2 1EZ, UK (fax: +44 1223 336 033; email: deposit@ccdc.cam.ac.uk or www: http://www.ccdc.cam.ac.uk).

Acknowledgements

This research is supported by the Program for Promoting University Academic Excellence from the Ministry of Education, Taiwan, Republic of China under the Contract PPAEU 91-E-FA04-2-4-(B).

References

[1] (a) P. Coppo, E.A. Plummer, L.D. Cola, Chem. Commun. (2004) 1774;
(b) S. Jung, Y. Kang, H.-S. Kim, Y.-H. Kim, C.-L. Lee, J.-J. Kim, S.-K. Lee, S.-K. Kwon, Eur. J. Inorg. Chem. (2004) 3415;
(c) J.D. Slinker, A.a. Gorodetsky, M.S. Lowry, J. Wang, S. Parker, R. Rohl, S. Bernhard, G.G. Malliaras, J. Am. Chem. Soc. 126 (2004) 2763;
(d) S. Lamansky, P. Djurovich, D. Murphy, F. Abdel-Razzaq, H.-F. Lee, C. Adachi, P.E. Burrows, S.R. Forrest, M.E. Thompson, J. Am. Chem. Soc. 123 (2001) 4304;
(e) M.E. Thompson, S. Lamansky, P.I. Djurovich, D. Murphy, F. Abdel-Razzaq, R. Kwong, S.R. Forrest, M.A. Baldo, P.E. Burrows, Patent US 20020034656A1.

[2] (a) A. Beeby, S. Bettington, I.D.W. Samuel, Z. Wang, J. Mater. Chem. 13 (2003) 80;
(b) C.-H. Yang, K.-H. Fang, C.-H. Chen, I.-W. Sun, Chem. Commun. (2004) 2232;
(c) V.V. Grushin, N. Herron, D.D. LeClous, W.J. Marshall, V.A. Petrov, Y. Wang, Chem. Commun. (2001) 1494.

[3] I.R. Laskar, S.-F. Hsu, T.-M. Chen, Polyhedron 24 (2005) 189.

[4] S. Lamansky, P. Djurovich, D. Murphy, F. Abdel-Razzaq, R. Kwong, I. Tsyba, M. Bortz, B. Mui, R. Bau, M.E. Thompson, Inorg. Chem. 40 (2001) 1704.

[5] M.E. Thompson, S. Lamansky, V. Adamovich, P.I. Djurovich, C. Adachi, R. Kwong, S.R. Forrest, M.A. Baldo, Patent US 2002/0182441 A1.

[6] G.M. Sheldrick, SAINT: Bruker Analytical X-ray Instrument Division, Madison, WI, 1998.

[7] G.M. Sheldrick, SHELXTL Programs, version 5.1; Bruker AXS GmbH, Karlsruhe Germany, 1998.

[8] J. Demas, G.A. Crosby, J. Phys. Chem. 75 (1971) 991.

[9] K.A. King, P.J. Spellane, R.J. Watts, J. Am. Chem. Soc. 107 (1985) 1431.

[10] F.O. Graces, K. Dedian, N.L. Keder, R.J. Watts, Acta Crystallogr., Sect. C 49 (1993) 1117.

[11] P.J. Hay, J. Phys. Chem. A 106 (2002) 1634.

[12] L.S. Sapochak, A. Padmaperuma, N. Washton, F. Endrino, G.T. Schmett, J. Marshall, D. Fogarty, P.E. Burrows, S.R. Forrest, J. Am. Chem. Soc. 123 (2001) 6300.

[13] (a) P.A. Lane, L.C. Palilis, D.F. O'Brien, C. Giebeler, A.J. Cadby, D.G. Lidzey, A.J. Campbell, W. Blau, D.D.C. Bradley, Phys. Rev. B 63 (2001) 235206;
(b) D.F. O'Brien, C. Giebeler, R.B. Fletcher, A.J. Cadby, L.C. Pallilis, D.G. Lidzey, P.A. Lane, D.D.C. Bradley, W. Blau, Synth. Met. 116 (2001) 379.